Shape selectivity in acidic zeolite catalyzed 2-pentene skeletal isomerization from first principles

Ya-Lan Wang[a,1], Xin-Xin Wang[a,1], Yi-An Zhu[a,*], Ka-Ke Zhu[a,*], De Chen[b], Xing-Gui Zhou[a]

[a] UNILAB, State Key Laboratory of Chemical Engineering, Shanghai Key Laboratory of Multiphase Materials Chemical Engineering, East China University of Science and Technology, Shanghai 200237, China
[b] Department of Chemical Engineering, Norwegian University of Science and Technology, N-7491 Trondheim, Norway

ARTICLE INFO

Keywords:
Isomerization
Zeolite catalysis
Density functional theory
Monomolecular reaction mechanisms
Ammonia adsorption
Scaling relation

ABSTRACT

Periodic density functional theory (DFT) calculations have been performed to examine the monomolecular reaction mechanism for 2-pentene skeletal isomerization catalyzed by acidic zeolite Beta, Mordenite, and ZSM-5. The use of periodic models allows consideration and analysis of zeolite steric constraints that occur within zeolite microspores. Three different reaction pathways, the "dimethylcyclopropane" (DMCP), methyl shift, and ethyl shift mechanisms, have been considered. The DMCP mechanism which includes rearrangement of protonated cyclopropane is proposed as the dominant reaction pathway, and the ring-opening step determines the overall reaction rate. Comparison of the effective energy barriers for 2-pentene isomerization over the three different zeolites reveals that large 12-ring channels of Beta and MOR have little steric hindrance effect on 2-pentene isomerization while small 10-ring of ZSM-5 significantly increases the reaction activation energy. Calculated results also indicate that the adsorption heat of ammonia is a good descriptor for the reactivity of zeolites without taking into account long-range dispersive forces. In contrast, linear scaling relations cannot be obtained by using the BEEF-vdW functional because van der Waals interactions between zeolites framework and guest molecules affects the energetics of the isomerization reaction and changes the transition state energy scaling relation in zeolite catalysis.

1. Introduction

Development of unleaded gasoline has been directed towards high octane quantity, high oxygen content, low aromatics, and low vapor pressure for economic and environmental reasons. As the most important parameter, octane number is a measure of knocking tendency when gasoline burns in an internal combustion engine. A higher octane number allows for a higher compression ratio of a gasoline engine without severe knocking [1], which in turn improves the engine efficiency and saves consumption of fuels. Basically, gasoline with a high octane quantity can be obtained by converting straight-chain paraffins into branch-chained paraffins [2,3], by dehydrogenation of saturated paraffins to olefins and aromatics [4], or by introducing additives such as methyl *tert*-butyl ether (MTBE) [5], among which skeletal isomerization of paraffins is most economical and effective [6].

Hydroisomerization is a class of important processes in the refining and petrochemical industry. Commercial *n*-paraffin hydroisomerization is often conducted over bifunctional catalysts comprising both metal centers (noble metals such as Pt or Pd) and Brønsted acid sites [7]. Very often, zeolites or zeotype materials that exhibit unique shape selective behavior make up the acidic components, producing desirable isomers and reducing cracking byproducts [8]. Both bimolecular and monomolecular reaction mechanisms have since been proposed to account for isomerization reactions [9–11]. The former was found to be more likely for *n*-butene isomerization [11], whereas for most larger homologues the monomolecular pathway is dominant [12]. In the monomolecular mechanism, *n*-alkanes are first dehydrogenated to corresponding *n*-alkenes on metal centers, which are subsequently protonated on acid sites to yield *n*-alkyl carbenium ions. Skeletal isomerization of carbenium ions produces *iso*-alkyl ions that desorb as *iso*-alkenes, and late hydrogenation of *iso*-alkenes produces isomers with various degrees of branching. Under ideal operation conditions, the fast (de)hydrogenation step can readily reach equilibrium, and the catalytic performance is determined largely by the acid component of the bifunctional catalyst. Hence, the identity of molecules, acid property, framework topology, and pore dimension of zeolites play a key role in determining the isomerization selectivity.

Isomerization of *n*-pentane to *iso*-pentene is an upstream reaction

for the production of *tert*-amyl methyl ether (TAME), a good oxygenate blend to gasoline due to its easy biodegradability. In contrast to MTBE, TAME has a low solubility in water and a low vapor pressure, which can effectively reduce air pollution. Pentene skeletal isomerization is a rather complex process, as side reactions such as double bond shift, dimerization, cracking, hydride transfer, oligomerization, and coke formation could affect the product distribution or catalyst lifetime. It is generally accepted that the acid strength required by these reactions decreases in the order cracking ≈ oligomerization > skeletal isomerization > double-bond isomerization [13]. Besides the need of moderate acid sites, the pore size is also an important factor influencing the *iso*-alkene selectivity in zeolite catalysis [14,15]. For instance, both Beta and Ferrierite (FER) zeolites can catalyze pentene isomerization to achieve an equilibrium conversion, but side reactions are negligible in the latter and a high selectivity to *iso*-pentene was observed [16], which was attributed to a restricted pore size of FER where *n*-pentene isomerization takes place exclusively by the monomolecular mechanism. Hence, a fundamental understanding of the corresponding reaction mechanism, kinetic features, as well as the origin of shape selectivity can provide crucial guidance for the selection of appropriate catalysts and reaction conditions to increase the selectivity for isomerization.

The analysis of reaction mechanism in zeolite catalysis has nowadays been greatly facilitated by theoretical modeling and simulation, as demonstrated by the mechanistic study of the MTO process [17]. The available theoretical investigations of *n*-paraffin isomerization usually start with the protonation of the dehydrogenated species, such as 2-pentene protonation in the skeletal isomerization of pentane [18], because the rate of *n*-pentene isomerization on a metal-free catalyst is the same as the overall reaction rate [19,20]. It was reported that *n*-pentene isomerizes mainly by the monomolecular mechanism on zeolites [21], which might occur via two possible pathways, namely, the one-step alkyl shift mechanism and the "protonated cyclopropane (PCP)" mechanism. These two mechanisms are hard to differentiate experimentally, thereby making theoretical investigation indispensable [18].

Previous [22] density functional theory (DFT) calculations, however, were based on cluster models to represent an acid site which is often insufficient to account for the confinement effect imposed by the pore geometry [23,24]. Although carbenium and carbenium-ion-like transition states are generally accepted as the key intermediates for the energetically favorable dimethyl-cyclopropane-mediated transformation, the extent to which primary and secondary carbenium ions could be stabilized by the anionic framework (and hence the origin of the shape selectivity) remains elusive and needs to be examined under periodic boundary conditions. Such a calculation has only been reported for small unidimensional pore zeolite ZSM-22 (TON) [18], and, no parallel studies have been performed so far to elucidate the dependence of the kinetics of 2-pentene isomerization on the framework topology.

In the current contribution, 2-pentene isomerization, as a paradigmatic example for the homologues, is investigated theoretically by carrying out periodic DFT calculations in three representative zeolite frameworks, namely, H-Beta (BEA, 12 × 12 × 12, interconnected 6.6 × 6.7 Å and 5.6 × 5.6 Å channels), H-Mordenite (MOR, 12 × 8, 6.5 × 7.0 Å channel with pocket void of 2.6 × 5.7 Å), and H-ZSM-5 (MFI, 10 × 10 × 10, interconnected 5.1 × 5.5 Å and 5.3 × 5.6 Å channels). A comparison is made to show the influence of pore geometry on the reaction kinetics, as the three zeolites have close Brønsted acidity. Given the complexity of the reaction network, we restrict this investigation to the two main reaction routes for the formation of monobranched isomers. A detailed reaction mechanism involving three possible reaction pathways, namely, the methyl shift, ethyl shift, and "protonated dimethyl-cyclopropane" (DMCP) pathways, will be considered in order to identify the kinetically most favorable route and to reveal the influence of anionic pore framework on the stability of the carbenium ion intermediates and transition states. Our calculated results indicate that the DMCP route is most likely to occur in all the three zeolites, and the detailed influences and implications of pore architectures will be discussed in the context of current studies.

2. Computational details

2.1. DFT calculation

Periodic DFT calculations were performed using the VASP Package [25–27]. The interactions between valence electrons and ion cores were represented by Blöchl's all-electron-like projector augmented wave method (PAW) with the plane wave basis set kinetic energy cutoff equal to 400 eV [28]. Exchange and correlation of the Kohn-Sham theory were treated with the generalized gradient approximation (GGA) in the formulation of the Perdew-Burke-Ernzerhof (PBE) functional and the Bayesian error estimation functional with van der Waals correlation (BEEF-vdW) [29–31]. In the latter functional, the long-range dispersion forces were accounted for by a semi-local approximation with an additional nonlocal correlation term, which proved to be of vital importance to accurately represent the physisorption of alkanes in microporous zeolites [29]. The Brillouin zone was sampled only at the Γ point by using the Monkhorst-Pack technique [32], and electronic occupancies were determined according to the Gaussian scheme with an energy smearing of 0.10 eV. A force threshold of 0.03 eV $Å^{-1}$ was used in geometry optimizations in which the positions of all atoms in the supercell were relaxed. The climbing-image nudged elastic band (CI-NEB) method [33] and minimum-mode following dimer method [34] and were utilized to locate transition states.

2.2. Zeolite model

Three zeotype topologies exhibiting different channel and cavity structures were employed to probe the detailed reaction mechanism for 2-pentene isomerization, including zeolite H-Beta, H-Mordenite, and H-ZSM-5. The BEA ($Si_{64}O_{128}$) and MFI ($Si_{96}O_{192}$) zeolite structures, in the all-silicon form, were first constructed by using a 1 × 1 × 1 unit cell. To avoid interactions between 2-pentene molecules in the periodic images, the primitive cell of MOR was doubled along the *c* axis to achieve a $Si_{48}O_{96}$ composition. The lattice constants were then optimized (12.70, 12.70, and 26.63 Å for BEA; 13.81, 13.81, and 15.19 Å for MOR; 20.53, 20.36, 13.66 Å for MFI) by using an energy cutoff of 600 eV and a force threshold of 0.01 eV/Å.

To construct a Brønsted acid site (bridging hydroxyl group) from the all-silicon porous framework, a silicon atom is replaced with an aluminum atom, with an adjacent oxygen atom saturated with hydrogen atom. According to crystallographic data [35], there are several types of tetrahedral sites (T-sites) for which Al can be substituted, and for each Al position there are four oxygen sites to which proton could be attached. In this work, a preliminary calculation of the physisorption heats and activation energies for the first elementary step was conducted to determine the most favorable substitution and establish the geometry of acidic zeolite models with one Brønsted acid site per unit cell.

The optimized H-Beta (Si/Al = 63), H-MOR (Si/Al = 47), and H-ZSM-5 (Si/Al = 95) geometries are shown schematically in Fig. 1 and the corresponding structural information is given in Table 1. For H-BEA, it was suggested that the Al(T9) − OH − Si(T4) or Al(T1) − OH − Si (T8) Brønsted acid site is energetically most favorable [36–38]. In our work, Al(T9) − OH − Si(T4) is calculated to be the most stable active site where the proton points towards the 12-membered large pore channel with a cross-section of 6.6 Å × 6.7 Å (The calculated results are summarized in Table S1 and Table S2). For MOR, the acid site formed with substitution of an Al atom for a Si atom at the T2 site is most stable among the four types of T-sites [39–41], in accordance with the model suggested by Benco et al. [42] where the resultant bridging hydroxyl group points towards the 12-MR pores (6.5 Å × 7.0 Å) (Table S3). As for H-ZSM-5, results from our work and other groups indicate that Al

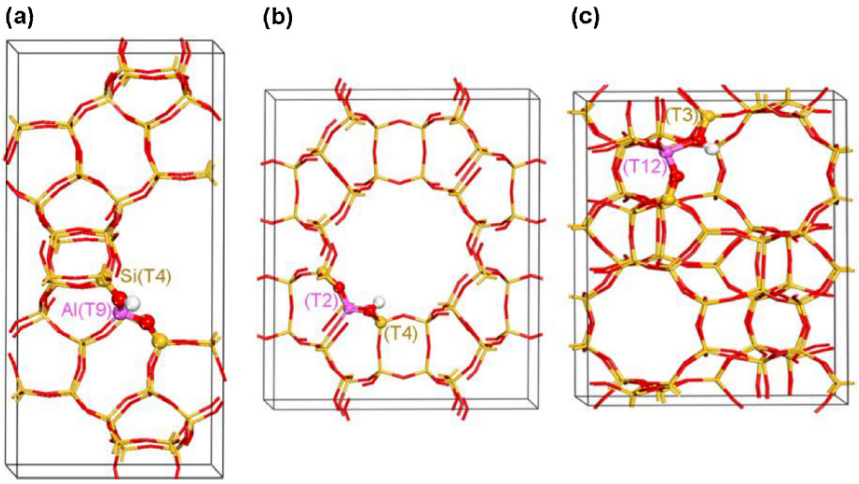

Fig. 1. Brønsted acid sites in the frameworks of (a) H-BEA, (b) H-MOR, and (c) H-ZSM-5 zeolites.

Table 1
Comparison of the structural properties of Brønsted acid sites in zeolites.

Framework	BEA	MOR	MFI
Formal composition	$Si_{64}O_{128}$	$Si_{48}O_{96}$	$Si_{96}O_{192}$
Acid site	Al(T9) − OH − Si (T4)	Al(T2) − OH − Si (T4)	Al(T12) − OH − Si (T3)
Ring sizes	12-ring	12-ring	10-ring
Pore size	6.6 × 6.7 Å	6.5 Å × 7.0 Å	5.3 Å × 5.6 Å
Si/Al ratio	63	47	95

(T12) − OH − Si(T3) is the most stable acid site and therefore chosen as the preferred acid site with the bridging OH group located in the 10-MR pores (5.3 Å × 5.6 Å) [43–45].

The adsorption energy of the C5 species in zeolites was calculated as

$$\Delta E_{ads} = E_{adsorbate/H-zeolite} - E_{adsorbate} - E_{H-zeolite} \quad (1)$$

Where $E_{adsorbate/H-zeolite}$ and $E_{H-zeolite}$ are the DFT total energies of H-zeolite with and without the adsorbate adsorbed, respectively, and $E_{adsorbate}$ is the total energy of an isolated C5 species. A negative ΔE_{ads} value indicates that adsorption is exothermic in nature. 2-pentene has two isomers, *trans*-2-pentene and *cis*-2-pentene. Here *trans*-2-pentene (P0) is selected as the reactant because it is ~ 0.05 eV lower in energy than *cis*-2-pentene.

3. Results and discussion

In *n*-pentane isomerization over metal/zeolite bifunctional catalysts, *n*-pentane dehydrogenates on metal surfaces first to form trans-2-pentene. The trans-2-pentene molecule is then protonated at the Brønsted acid sites to generate two possible alkoxides, pent-2-oxide and pent-3-oxide. After that, the two alkoxides can isomerize via the methyl shift (MS), ethyl shift (ES), and dimethylcyclopropane (DMCP) mechanisms to yield different monobranched alkoxide isomers, which in turn desorbs via deprotonation as 2-methyl-1-butene or 2-methyl-2-butene. Finally, the two *iso*-pentenes are hydrogenated on metal surfaces to produce 2-methyl-butane. During the whole process, formation of pentenium and isopentenium are considered as the most important step. The nature of carbenium ions and their interactions with pore wall could affect the reaction rate and change the isomer-to-cracking ratio. Therefore, in the first part of the present work, we focus on all the three skeletal isomerization mechanisms for trans-2-pentene isomerization in H-BEA to identify the dominant reaction pathway, as displayed in Scheme 1.

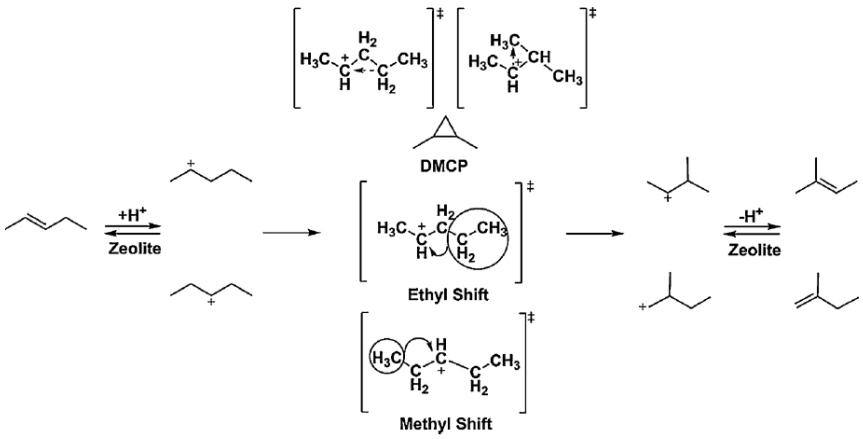

Scheme 1. Zeolite-catalyzed isomerization of 2-pentene by the methyl shift (MS), ethyl shift (ES), and dimethylcyclopropane (DMCP) mechanisms.

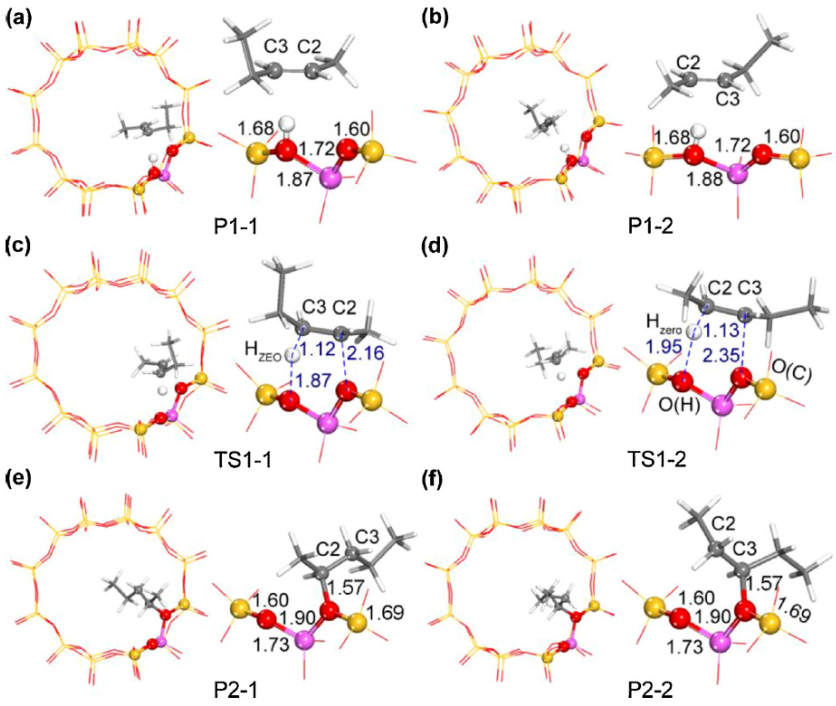

Fig. 2. Geometrical structures of the initial P1-1 (a), P1-2 (b), transition states TS1-1 (c), TS1-2 (d) and intermediates P2-1 (e), P2-2 (f) for the transformation of physisorbed 2-pentene to alkoxides intermediates within the BEA zeolite channels. The interatomic distances are given in Å.

3.1. Adsorption and protonation of trans-2-pentene in BEA zeolite

Adsorption of *trans*-2-pentene is the first step in the skeletal isomerization mechanism. The two lowest-energy adsorption configurations (P1-1 and P1-2) of *trans*-2-pentene are shown in Fig. 2a and b, respectively. One can see from Fig. 2 that the *trans*-2-pentene molecule is not covalently bonded to the BEA zeolite channels, and the measured interatomic distances between C2 (or C3) and the acidic proton (H_{zeo}) are in the range of 2.0–2.2 Å. Furthermore, the optimized bond lengths and angles of the physisorbed 2-pentene are almost identical to those in the gas-phase *trans*-2-pentene. The C2 = C3 double bond is aligned parallel to the two oxygen atoms involved in the acid site to achieve a π-complex, which would subsequently be converted via a ring-like transition state to generate two surface alkoxides. The adsorption energies of 2-pentene in the most stable configuration (P1-1) are calculated to be –0.35 and –0.84 eV by using the PBE and BEEF-vdW functionals, respectively, indicating van der Waals interaction plays a key role in stabilizing the adsorption configurations of 2-pentene inside the zeolite framework.

Upon adsorption, two distinct products, pent-2-oxide (P2-1) and pent-3-oxide (P2-2), may be produced because protonation could take place on either side of the double bond. As the reaction proceeds, the H_{zeo}–O bond is broken and the proton is transferred to the C3 (or C2) atom. Meanwhile, the C2 = C3 double bond is stretched from 1.35 Å to 1.45 Å in both transition state geometries (see Fig. 2c and d). In the final states, the C2–O and C3–O bonds are eventually formed at the adjacent bridging O atom to the one initially coordinated to the proton, with the bond lengths being 1.57 Å (see Fig. 2e and f).

The calculated activation energies for the C2–O bond formation (0.53 eV by PBE and 0.57 eV by BEEF-vdW) are lower than those for the C3–O bond formation (0.58 eV by both PBE and BEEF-vdW), suggesting that the formation of pent-2-oxide is kinetically more favorable. Our calculated results in 12-ring channel system compare closely to the data obtained by Demuth et al. who predicted an activation energy of 52 kJ/mol (0.54 eV) for 2-pentene chemisorption in ZSM-22 zeolite that has 10-membered rings, implying that the pore dimensions and topologies have a negligible effect on the kinetics of protonation of *trans*-2-pentene. Given the fact that the resulting pent-2-oxide is more stable than pent-3-oxide, the chemisorption of *trans*-2-pentene to produce pent-2-oxide is favored from both kinetic and thermodynamic considerations.

The variations between the transition states and chemisorption state energies can be rationalized as follows. First, in the *trans*-2-pentene structure, the hyper-conjugation effect between the double bond and the methyl group is stronger than that between the double bond and the ethyl group. Consequently, the stronger hyper-conjugation effect makes the C2 atom which is directly connected to the methyl group more difficult to be protonated. Second, when the C–O bond is formed in alkoxides, the C3 atom that is bonded to two ethyl groups must experience larger steric hindrance when the C2 atom approaches the bridging O atom, thus making the formation of pent-3-oxide more space-demanding. Nevertheless, the small differences in energy barrier and chemisorption energy show that formation of both the alkoxides is possible and they supposedly have close surface coverages under reaction conditions.

3.2. Skeletal isomerization mechanisms of pent-2-oxide and pent-3-oxide in BEA zeolite

3.2.1. Skeletal isomerization via the DMCP pathway

As aforementioned, monomolecular skeletal isomerization might occur by either the protonated cyclopropane (PCP) or the one-step alkyl shift mechanism. The PCP mechanism was first proposed by Brouwer et al. [46] for isomerization in liquid super-acids and later by Weitkamp [47] for skeletal isomerization in zeolites. Since relatively stable secondary and tertiary carbenium ions were postulated to appear during the course of the reaction [48], this mechanism was suggested to be more likely for the isomerization of linear *n*-alkenes. Rigby et al. [23] used quantum chemical calculations coupled with the cluster approach to examine the energetics of the skeletal isomerization of *n*-butene via the methyl shift pathway and found that the calculated activation

energies for the isomerization of *n*-butyl alkoxide are quite close to those for larger *n*-alkoxides, which is in conflict with experimental observations. Consequently, authors concluded that other reaction pathways need to be considered to account for n-butene isomerization [23].

It is important to note that the cluster approach used in many early studies [49,50] does not aim to model the zeolite framework in an accurate way but focuses only on the zeolite catalytic site [51,52]. Therefore, the possibility cannot be disregarded that such a calculation could make a wrong predication about the reaction mechanism. As an alternative, the periodic DFT calculations could be a better choice because both the short- and long-range interactions between zeolite frameworks and carbenium ions can possibly be taken into consideration. The work by Demuth et al. [18] is the first attempt to study the isomerization of a linear alkene by considering periodic boundary conditions, although the long-range London dispersion forces are not explicitly accounted for in their calculations.

Here the DMCP pathway is revisited using the periodic model so as to explore how the reaction kinetics could be influenced by van der Waals interactions imposed by the pore walls. The reaction mechanism for pent-2-oxide isomerization in acidic zeolites via the protonated DMCP pathway is illustrated in Scheme 1, and the geometries of the transition states and intermediates are presented in Fig. 3. Upon chemisorption of 2-pentene, the more stable alkoxide, pent-2-oxide, is assigned as the initial state for the subsequent isomerization reaction. At the first saddle point, a secondary carbenium-like transition state (TS2-DMCP) results when the cyclopropane ring (C2–C3–C4) is progressively closed, where a hydrogen atom is simultaneously detached from the C4 atom to restore the acid site. When this proton back donation is complete, the formation of an adsorbed DMCP intermediate (P3-DMCP) at a Brønsted acid site is finally achieved. With the progression of the reaction, the DMCP molecule is rotated by approximately 90° in the C2–C3–C4 plane, in order for the C3 atom to interact with the proton (TS3-DMCP). At the second saddle point, the C2–C3–C4 cyclopropane ring opening takes place, accompanied by the C3–C4 and H–O(H) bond cleavage, giving thus rise to another secondary carbenium-like transition state. The origin of this transformation lies in the Markovnikov Rule [53] that hydrogen prefers to be bonded to carbon atoms having higher C–H coordination numbers. In the final state (P4-DMCP), the pentyl group is positioned perpendicularly to the 12-membered ring channel to generate a secondary isopentyl oxide and the resulting C4–O(H) bond length of 1.58 Å is slightly longer than the C2–O bond (1.57 Å) in the pent-2-oxide. The detailed structural information is included in Table S5.

3.2.2. Skeletal isomerization via the alkyl shift pathway

Previous quantum chemical studies demonstrated that the alkyl shift mechanism is also possible for the skeletal isomerization of *n*-pentane by using a cluster model [23]. For the purposes of identifying the dominant reaction pathway, the alkyl shift mechanism is explored in this work by using periodic DFT calculations. In the methyl and ethyl shift pathways, the pent-3-oxide and pent-2-oxide are taken as the initial states, respectively, and in both the transition states (TS2-MS and TS2-ES) three carbon atoms are arranged in a triangular fashion, which eventually gives rise to the formation of a primary isopentyl oxide [P4-MS(ES)], as can be seen in Fig. 4. In the TS2-MS configuration, a methyl group (C1) is shifted from the C2 atom to the C3 atom, with the C1–C2 interatomic distance increased from 1.53 Å to 1.96 Å and the C1–C3 bond length decreased from 2.53 Å to 1.67 Å, while in the TS2-ES configuration an ethyl group (C4–C5) moves away from the C3 atom and towards the C2 atom as an ethyl ion. In the final state, the pentyl group is perpendicular to the 12-membered ring channel to generate the pent-iso-oxide, and the resultant C3(C2)–O(H) bond has a bond length of 1.53 Å. The detailed configurational information is presented in the Table S6.

The calculated energy change associated with the alkyl shift mechanism is invariably positive, regardless of the exchange-correlation functional used, i.e., the initial states are energetically more favorable than the final state, which can be explained by the different stability of the primary and secondary alkoxides. Furthermore, the calculated activation energy for methyl shift pathway (PBE by 1.09 eV and BEEF-vdW by 1.06 eV) is slightly lower than that for the ethyl shift pathway (PBE by 1.10 eV and BEEF-vdW by 1.09 eV), which is contrary to the general belief for the gas-phase molecules that because of the lower stability of the methyl ion the formation of a methyl group is kinetically much slower. The origin of the activation energy difference observed in our work lies in the fact that the pent-2-oxide is more stable than the pent-3-oxide within zeolitic channels, which can be attributed to the stabilization effect arising from London dispersion attractions. On the other hand, the geometries of the two corresponding transition states resemble the same final state [P4-MS(ES)] and have very close energies. As a consequence, the ethyl shift pathway needs more energy to surmount the transition state.

3.3. Desorption of iso-pentene in BEA zeolite

Once skeletal isomerization is achieved, the resultant pent-iso-oxide [P4-ME(ES) and P4-DMCP] needs to desorb from the Brønsted site to yield a molecular *iso*-pentene, leaving behind a restored acid site. According to the three aforementioned isomerization pathways,

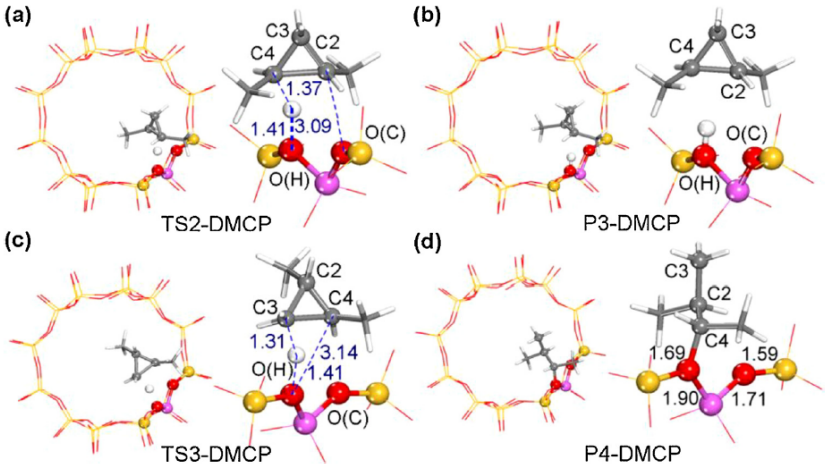

Fig. 3. Geometrical structures of transition states TS2-DMCP (a), TS3-DMCP (c) and intermediates P3-DMCP (b), P4-DMCP (d) for pent-2-oxide isomerization by the DMCP mechanism in BEA zeolite. The interatomic distances are given in Å.

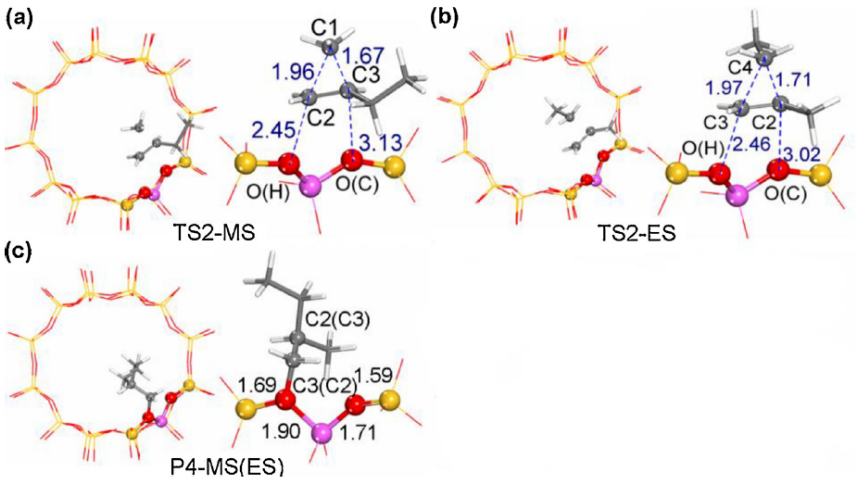

Fig. 4. Geometrical structures of the transition states TS2-MS (a), (TS2-ES) (b) and intermediate P4-MS(ES) (c) for pent-2-oxide isomerization by the methyl or ethyl shift mechanism in BEA zeolite. The interatomic distances are given in Å.

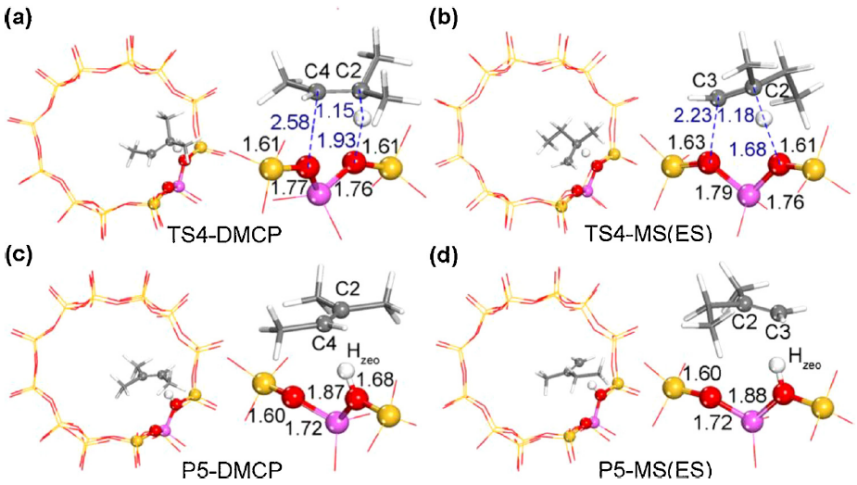

Fig. 5. Geometrical structures of the transition states TS-DMCP (a), TS-MS(ES) (b) and final states P5-DMCP (c), P5-MS(ES) (d) for formation of *iso*-pentene via deprotonation in BEA zeolite. The interatomic distances are given in Å.

desorption products of the DMCP and alkyl shift would be a secondary and a primary *iso*-pentene, respectively. The structural parameters in the configurations of the transition states and products involved are summarized in Table S7. Fig. 5 depicts the geometries of the transition states and final states for desorption of *iso*-pentene in BEA zeolite. In the TS4-DMCP configuration, the C4–O(H) bond is broken, and the interatomic distance is elongated to 2.58 Å. By comparison, the C3–O(H) bond length in the TS4-MS(ES) configuration is measured to be 2.23 Å, thereby leading to a significantly different interaction between the organic species and zeolite framework. In the P5-DMCP and P5-MS(ES) final states, 2-methyl-2-butene and 2-methyl-1-butene are weakly adsorbed at the Brønsted site, respectively, and upon completion of the overall catalytic cycle the acidic photon is transferred from one bridging oxygen atom to its neighboring counterpart.

The calculated physisorption energy of 2-methyl-1-butene is less negative than that of 2-methyl-2-butene, which is consistent with the normal idea that the more double atoms connected to the alkyl group, the more stable is the alkene. Furthermore, the desorption barrier for the alkyl shift pathway is much higher than that for the DMCP mechanism, which is due to the formation of the less stable primary carbenium ion-like transition state in the former.

3.4. Energetic analysis of 2-pentene isomerization in BEA zeolite

3.4.1. Contribution from van der Waals interactions

To elucidate the reaction mechanism for *trans*-2-pentene isomerization and reveal the key role of van der Waals interactions in determining the dominant reaction pathway, both the PBE and BEEF-vdW functionals were applied in this work. Calculated results indicate that while similar geometries of intermediates and transition states can be obtained with both the functionals, there is a profound difference in the energetics. The energy profiles for *trans*-2-pentene isomerization catalyzed by acidic H-BEA via the three possible pathways are presented in Fig. 6. Both the PBE and BEEF-vdW results indicate that the DMCP pathway has the lowest apparent activation energy and therefore dominates the kinetics of the overall reaction, which can be attributed to the presence of the secondary carbocation-like transition states that is more stable than the primary carbocation-like transition states in the alkyl shift mechanisms.

On the other hand, the calculated physisorption energy of 2-pentene by using the BEEF-vdW functional is –0.84 eV, much more negative than the data obtained by PBE and in accord with the results obtained by Nguyen et al. [54] which is around –80 kJ/mol when van der Waals interactions were taken into account. Furthermore, all the energetics obtained by using the BEEF-vdW functional become more negative by around 0.50 eV, signifying that the actual bonding strengths between

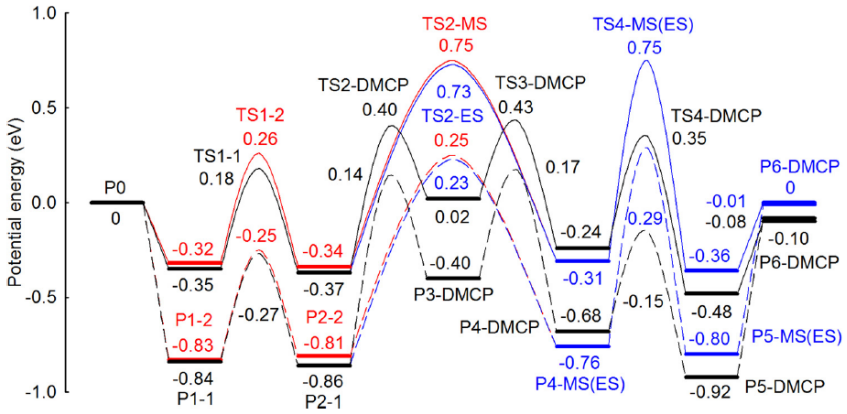

Fig. 6. Potential energy diagrams for *trans*-2-pentene isomerization catalyzed by acidic H-BEA via three possible reaction pathways, using PBE (solid line) and BEEF-vdW functionals (dashed line). The DMCP, methyl shift, and ethyl shift mechanisms are colored black, red, and blue, respectively.

the organic species and the zeolite framework are much greater than the PBE functional predicts. It is well accepted that the structural stability of the organic species may influence the reactivity and selectivity of reactions in zeolites. In our work, while the introduction of van der Waals interactions does not change the dominant reaction pathway, the activation energy for the overall reaction is apparently changed.

3.4.2. Effective reaction barrier

Since van der Waals interactions are particularly important in a quantitative description of the kinetics of 2-pentene isomerization in zeolites, the energetic span theory [55–57] combined with the DFT results obtained by the BEEF functional is employed to predict with reasonable accuracy the effective reaction barrier for the overall isomerization reaction. The energetic span theory was proposed by Kozuch and Shaik who believed that the effective reaction barrier (E_a^{eff}) for an overall reaction is the energy difference between two rate-determining states in the overall reaction pathway rather than the reaction barrier for the rate-determining step:

$$E_a^{eff} = \begin{cases} G_{TDTS} - G_{TDI} & \text{if TDTS appears after TDI} \\ G_{TDTS} - G_{TDI} + \Delta Gr & \text{if TDTS appears before TDI} \end{cases} \quad (2)$$

where TDTS represents the rate-determining transition state, TDI stands for the rate-determining intermediate, and ΔGr is the Gibbs energy change for the reaction.

Under the reaction conditions (T = 573.15 K and P = 101,325 Pa), the simulated Gibbs free energy diagram of 2-pentene isomerization in BEA zeolite using the BEEF-vdW functional is shown in Fig. 7, and the corresponding potential energy diagrams are also given for comparison. From the figure, one can see that the calculated reaction Gibbs energy change is –0.08 eV (ΔGr = –0.08 eV) for the DMCP mechanism. For the alkyl shift mechanism, ΔGr turns to 0.02 eV under the same reaction conditions. By using the energetic span theory, the calculated effective reaction barrier for the dominant DMCP pathway is 1.04 eV, and for the methyl shift and ethyl shift mechanisms the data are both 1.18 eV. Since the effective energy barriers for the three reaction pathways are comparable, all of them may contribute to the reaction kinetics, although the DMCP pathway is kinetically most relevant. Experimentally, the key intermediates, such as pent-2-oxide, pent-3-oxide, and the desorbed isopentene, have been observed through in situ 13-labeled n-pentane isomerization NMR measurements on solid acid sulfated zirconia catalyst [21], showing that monomolecular mechanism through these intermediates is the most likely reaction pathway. A monomolecular bifunctional mechanism has been suggested as the preferred route for reaching high isomerization selectivity over MOR by experiments as well [58]. From the Gibbs free energy diagram, one can also see that the ring-opening step (the formation of TS3-DMCP) that involves the rate-determining transition state is the rate-determining step in the DMCP pathway.

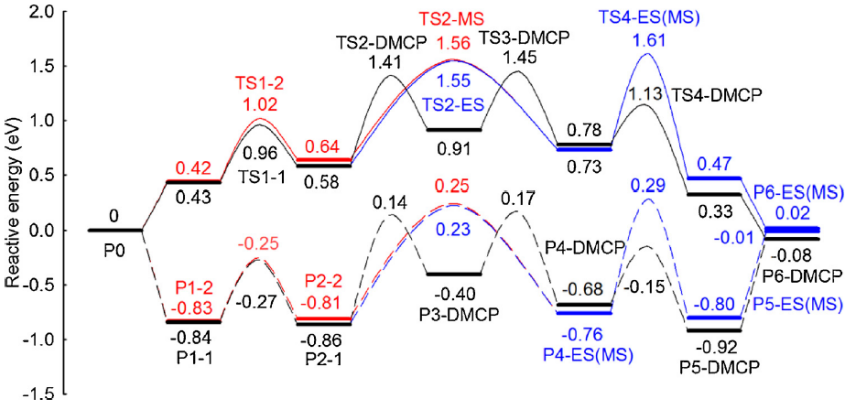

Fig. 7. Energy profiles for *trans*-2-pentene isomerization catalyzed by acidic H-BEA via three possible pathways, using the BEEF-vdW functional, at 0 K (dashed line) and 573 K (solid line). The DMCP, methyl shift, and ethyl shift mechanisms are colored black, red, and blue, respectively.

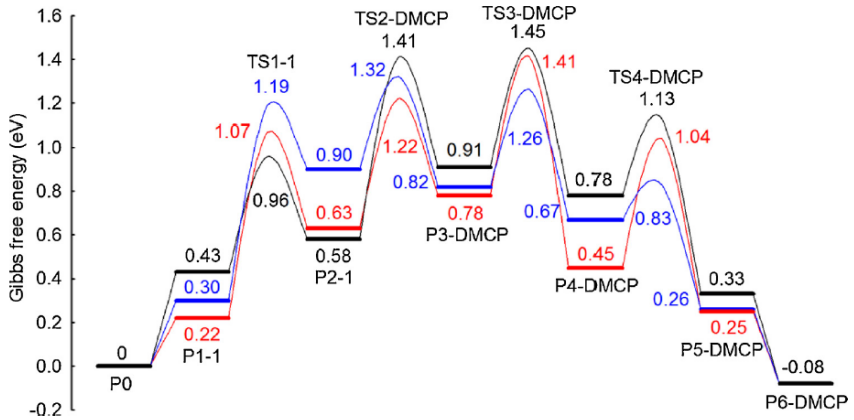

Fig. 8. Gibbs free energy diagrams for *trans*-2-pentene isomerization catalyzed by acidic ZSM-5 (in red), MOR (in blue), and BEA (in black) via the DMCP pathway, using BEEF-vdW functional, at 573 K and 101,325 Pa.

3.5. Effect of zeolite framework on the reaction kinetics

To further analyze the effect of zeolite framework on the kinetics of 2-pentene isomerization, the dominant DMCP pathway was also examined in other two zeolites, MOR and ZSM-5, by using both the PBE and the BEEF-vdW functionals. With van der Waals forces considered, the calculated physisorption energies of *trans*-2-pentene are –0.99 eV over H-MOR and –1.06 eV over H-ZSM-5, which compare closely to the work by Nguyen et al. [54] (–85 kJ/mol in H-MOR and –95 kJ/mol in H-ZSM-5). It can therefore be deduced that the van der Waals interactions perceived by 2-pentene are not identical in different zeolite frameworks. The smaller zeolite channels exert greater long-range dispersive attractions to the C5 species.

The Gibbs free energy diagrams for *trans*-2-pentene isomerization catalyzed by acidic H-BEA, H-MOR, and H-ZSM-5 via the DMCP pathway using BEEF-vdW functional at 573 K is shown in Fig. 8. According to the energetic span theory, the calculated reaction Gibbs energy change and effective reaction barrier over H-MOR zeolites are –0.08 eV and 1.02 eV.

As for H-ZSM-5 zeolite, the effective reaction barrier (1.19 eV) is the highest among those for the three zeolites, which can be explained by the idea that isomerization reaction of *trans*-2-pentene over BEA and MOR zeolite occur in 12-memberd rings, without obvious space steric effect arising from small zeolite channels. For ZSM-5 zeolite, however, the zeolite channel has smaller 10-membered rings, limiting the degree of freedom in the transition states and increasing its activation energy accordingly. Hence, the catalytic performance could be quite different at active sites having crystallographically different local environments, and our periodic models represent a good system to study the effect of van der Waals interactions on the catalytic activity of zeolites for 2-pentene isomerization.

Although experimental kinetic studies have been carried out to estimate the apparent activation energies over Pt/Mordenite (111.8 kJ/mol) [12], Pt/Beta (124 kJ/mol) [59], as well as Pt/ZSM-22 (128 kJ/mol) [59], these values, however, should not be compared with our theoretical predications because they contain contributions from dehydrogenation and protonation steps, as suggested by Iglesia et al. [60,61] and Chica and Corma [62] for hydroisomerization of n-hexane and n-octane proceeding through the monomolecular pathway, respectively. A more rigorous experimental estimation of the intrinsic activation barrier for n-pentane hydroisomerization is yet to be achieved.

3.6. Linear transition state enthalpy scaling relations

Experimentally, the adsorption heat of ammonia (ΔH_{NH_3}) is often used as a measure of the Brønsted acid strength. Wang et al. [63] have performed periodic DFT calculations to find that the ΔH_{NH_3} can be considered as a descriptor to establish scaling relations for energies of intermediates and transition states and can therefore be used to describe the reactivity of acid sites. The question that now arises is whether this quantity can also be used to correlate with the reactivity of 2-pentene isomerization in zeolites.

According to the Gibbs free energy diagrams shown in Fig. 8, the ring opening step is the rate-determining step in the DMCP pathway over BEA and ZSM-5 zeolite. For H-MOR, formation of adsorbed DMCP and ring opening steps jointly determine the overall reaction rate. Hence, the enthalpies of the transition states for the ring opening step in the three zeolites are plotted as a function of the ΔH_{NH_3}, as shown in Fig. 9. In Fig. 9, a very good linear scaling relation is established on the basis of the data obtained from the PBE calculations, indicating that the ΔH_{NH_3} captures the influence of acid strength on the energetics for the transition states of the rate-determining step and the deprotonated acid sites, i.e., ΔH_{NH_3} is a good descriptor for the reactivity of acid sites in

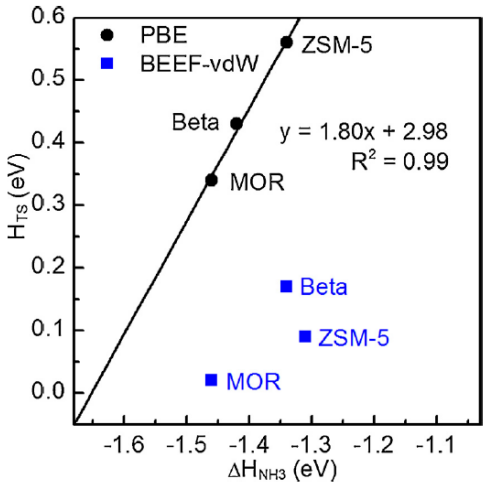

Fig. 9. Linear transition state enthalpy scaling relation for the rate-limiting ring opening step in the DMCP mechanism of *trans*-2-pentene isomerization, by using the PBE and BEEF-vdW functionals.

zeolites without considering van der Waals interactions.

However, the scaling between the same two quantities obtained by using the BEEF-vdW functional cannot give a straight line, merely because ammonia is such a small molecule that the ΔH_{NH_3} cannot provide any information about the surrounding environment of acid sites and shape-selective properties of zeolitic catalysts. On the other hand, the introduction of van der Waals forces has a significant effect on the transition state enthalpies of the rate-determining step. As a consequence, the linear transition state enthalpy scaling relation can no longer be obtained and identification of a descriptor that can capture the shape-selective properties of porous catalysts is highly desired. Nevertheless, the descriptor-based approach (ΔH_{NH_3} as descriptor, neglecting van der Waals interactions) could be preliminarily used as the first step of rational catalyst design to establish scaling relations and predict the activity of different zeolite catalysts.

Indeed, previous kinetic studies for relatively large n-hexane hydroisomerization has demonstrated that the acid strength (in terms of deprotonation energy) plays a center role in deciding the intrinsic catalytic activity in the rate-determining skeletal isomerization step [60,61], and similar scenario can be expected for n-pentene. N-pentene is relatively small and is more likely to be affected by acidity rather than pore dimension of zeolites. Still, the dispersion energy and attraction between positively charged pentyl ions and negatively charged pore walls bring about additional stability of the carbenium ions, which further lowers the intermediates and transition states. More pertinent probe molecule based descriptor is under investigation and will be reported in the future.

4. Conclusions

DFT-GGA calculations have been performed to study the skeletal isomerization of *trans*-2-pentene catalyzed by BEA, MOR, and ZSM-5 zeolites. Three skeletal isomerization pathways, namely, the DMCP, methyl shift, and ethyl shift pathways have been considered and proved to be likely under various reaction conditions. The DMCP mechanism is found to be the dominant pathway because of the formation of more stable secondary carbenium-like transition states, and the ring opening step likely dominates the kinetics of the overall reaction. According to the energetic span theory, the effective reaction barrier for the DMCP pathway over ZSM-5 zeolite is ~ 0.2 eV higher than those over BEA and MOR zeolites, which can be explained by the insignificant steric hindrance within large 12-ring channels of Beta and MOR. Therefore, the smaller the channels, the larger is the effect of van der Waals forces. Calculated results also indicate that the ΔH_{NH_3} is a good descriptor for the reactivity of zeolites without taking into account long-range dispersive forces. In contrast, linear scaling relations cannot be obtained by using the BEEF-vdW functional because van der Waals interactions between zeolites framework and organic species greatly affects the energetics of the isomerization reaction and change the transition state energy scaling relations in zeolite. These results provide conceptual consideration for understanding the effects of local environment, zeolite channel size and connectivity on the reaction kinetics.

Acknowledgements

This work is supported by the Natural Science Foundation of China (21473053, 21576082, 91645122, and U1663221), the National Key Research and Development Program of China (2018YFB0604700), and the Fundamental Research Funds for the Central Universities (222201718003). The computational time provided by the Notur project is highly acknowledged.

Appendix A. Supplementary data

Supplementary material related to this article can be found, in the online version, at doi:https://doi.org/10.1016/j.cattod.2018.06.009.

References

[1] R.L. Speth, E.W. Chow, R. Malina, S.R.H. Barrett, J.B. Heywood, W.H. Green, Environ. Sci. Technol. 48 (2014) 6561–6568.
[2] C. Travers, N. Essayem, M. Delage, S. Quelen, Catal. Today 65 (2001) 355–361.
[3] R. Yadav, A. Sakthivel, Appl. Catal. A: Gen. 481 (2014) 143–160.
[4] T.G. Kaufmann, A. Kaldor, G.F. Stuntz, M.C. Kerby, L.L. Ansell, Catal. Today 62 (2000) 77–90.
[5] A.V. Wezel, L. Puijker, C. Vink, A. Versteegh, Pd. Voogt, Chemosphere 76 (2009) 672–676.
[6] A. Chica, A. Corma, J. Catal. 187 (1999) 167–176.
[7] C.M. López, V. Sazo, P. Pérez, L.V. García, Appl. Catal. A: Gen. 372 (2010) 108–113.
[8] K.J. Chao, H.C. Wu, L.J. Leu, Appl. Catal. A: Gen. 143 (1996) 223–243.
[9] E. Blomsma, J.A. Martens, P.A. Jacobs, J. Catal. 159 (1996) 323–331.
[10] M.J. Wulfers, F.C. Jentoft, J. Catal. 330 (2015) 507–519.
[11] J. Čejka, B. Wichterlová, P. Sarv, Appl. Catal. A: Gen. 179 (1999) 217–222.
[12] H. Liu, G.D. Lei, W.M.H. Sachtler, Appl. Catal. A: Gen. 137 (1996) 167–177.
[13] A. Corma, B.W. Wojciechowski, Catal. Rev. 24 (1982) 1–65.
[14] P. Mériaudeau, A.V. Tuan, N.L. Hung, G. Szabo, Catal. Lett. 47 (1997) 71–72.
[15] J. Houžvička, S. Hansildaar, V. Ponec, J. Catal. 167 (1997) 273–278.
[16] K. Föttinger, G. Kinger, H. Vinek, Appl. Catal. A: Gen. 249 (2003) 205–212.
[17] C.M. Wang, Y.D. Wang, Y.J. Du, G. Yang, Z.K. Xie, Catal. Sci. Technol. 5 (2015) 4354–4364.
[18] T. Demuth, X. Rozanska, L. Benco, J. Hafner, R.A. van Santen, H. Toulhoat, J. Catal. 214 (2003) 68–77.
[19] J.W. Niemantsverdriet, R.A. van Santen, Chemical Kinetics and Catalysis, Plenum Press, London, 1995.
[20] H. Noguchi, E. Yoda, N. Ishizawa, J.N. Kondo, A. Wada, H. Kobayashi, K. Domen, J. Phys. Chem. B 109 (2005) 17217–17223.
[21] M.V. Luzgin, A.G. Stepanov, V.P. Shmachkova, N.S. Kotsarenko, J. Catal. 203 (2001) 273–280.
[22] A. Soualah, J.L. Lemberton, L. Pinard, M. Chater, P. Magnoux, K. Moljord, Appl. Catal. A: Gen. 336 (2008) 23–28.
[23] A.M. Rigby, M.V. Frash, J. Mol. Catal. A: Chem. 126 (1997) 61–72.
[24] Y.H. Guo, M. Pu, L.Y. Liu, H.F. Li, B.H. Chen, Comp. Mater. Sci. 42 (2008) 179–185.
[25] G. Kresse, J. Hafner, Phys. Rev. B 47 (1993) 558–561.
[26] G. Kresse, J. Furthmüller, Comp. Mater. Sci. 6 (1996) 15–50.
[27] G. Kresse, J. Furthmüller, Phys. Rev. B 54 (1996) 11169.
[28] G. Kresse, D. Joubert, Phys. Rev. B 59 (1999) 1758–1775.
[29] R.Y. Brogaard, P.G. Moses, J.K. Nørskov, Catal. Lett. 142 (2012) 1057–1060.
[30] C.M. Nguyen, B.A. De Moor, M.F. Reyniers, G.B. Marin, J. Phys. Chem. C 116 (2012) 18236–18249.
[31] J. Wellendorff, K.T. Lundgaard, A. Møgelhøj, V. Petzold, D.D. Landis, J.K. Nørskov, T. Bligaard, K.W. Jacobsen, Phys. Rev. B 85 (2012) 5826–5831.
[32] H.J. Monkhorst, J.D. Pack, Phys. Rev. B 13 (1976) 5188–5192.
[33] G. Henkelman, B.P. Uberuaga, H. Jónsson, J. Chem. Phys. 113 (2000) 9901–9904.
[34] G. Henkelman, H. Jónsson, J. Chem. Phys. 111 (1999) 7010–7022.
[35] J.M. Newsam, M.M.J. Treacy, W.T. Koetsier, C.B. de Gruyter, Proc. R. Soc. Lond. A 420 (1988) 375–405.
[36] M. Boronat, A. Corma, M. Renz, G. Sastre, P.M. Viruela, Chem. Eur. J. 11 (2005) 6905–6915.
[37] H. Fujita, T. Kanougi, T. Atoguchi, Appl. Catal. A: Gen. 313 (2006) 160–166.
[38] A. Andersen, N. Govind, L. Subramanian, Mol. Simulat. 34 (2008) 1025–1039.
[39] A. Simperler, R.G. Bell, M.W. Anderson, J. Phys. Chem. B 108 (2004) 7142–7151.
[40] A. Jansen, V. Ruangpornvisuti, J. Mol. Catal. A: Chem. 363 (2012) 171–177.
[41] L. Díaz, A. Sierraalta, M.A.C. Nascimento, R. Añez, J. Phys. Chem. C 117 (2013) 5112–5117.
[42] L. Benco, T. Bucko, J. Hafner, J. Catal. 277 (2011) 104–116.
[43] D.C. Tranca, N. Hansen, J.A. Swisher, B. Smit, F.J. Keil, J. Phys. Chem. C 116 (2012) 23408–23417.
[44] V. Shapovalov, A.T. Bell, J. Phys. Chem. C 114 (2010) 17753–17760.
[45] T. Maihom, P. Pantu, C. Tachakritikul, M. Probst, J. Limtrakul, J. Phys. Chem. C 114 (2010) 7850–7856.
[46] D.M. Brouwer, H. Hogeveen, Electrophilic Substitutions at Alkanes and in Alkylcarbonium Ions, Progress in Physical Organic Chemistry, John Wiley & Sons, Inc, 2007, pp. 179–240.
[47] J. Weitkamp, Ind, Eng. Chem. Prod. Res. Dev. 21 (1982) 550–558.
[48] M.V. Frash, V.B. Kazansky, A.M. Rigby, R.A. van Santen, J. Phys. Chem. B 101 (1997) 5346–5351.
[49] M.V. Frash, R.A. van Santen, Top. Catal. 9 (1999) 191–205.
[50] M.V. Frash, V.B. Kazansky, A.M. Rigby, R.A. van Santen, J. Phys. Chem. B 102 (1998) 2232–2238.
[51] A.M. Vos, X. Rozanska, R.A. Schoonheydt, R.A. van Santen, F. Hutschka, J. Hafner, J. Am. Chem. Soc. 123 (2001) 2799–2809.
[52] X. Rozanska, R.A. van Santen, T. Demuth, F. Hutschka, J. Hafner, J. Phys. Chem. B 107 (2003) 1309–1315.
[53] G. Jones, J. Chem. Edu. 38 (1961) 297.
[54] C.M. Nguyen, B.A. De Moor, M.F. Reyniers, G.B. Marin, J. Phys. Chem. C 115 (2011) 23831–23847.
[55] S. Kozuch, S. Shaik, J. Am. Chem. Soc. 128 (2006) 3355–3365.
[56] S. Kozuch, S. Shaik, Acc. Chem. Res. 44 (2011) 101–110.
[57] S. Kozuch, J.M.L. Martin, ACS Catal. 1 (2011) 246–253.
[58] N. Essayem, Y.B. Taârit, C. Feche, P.Y. Gayraud, G. Sapaly, C. Naccache, J. Catal. 219 (2003) 97–106.
[59] T. Matsuda, K. Watanabe, H. Sakagami, N. Takahashi, Appl. Catal. A: Gen. 242 (2003) 267–274.
[60] J. Macht, R.T. Carr, E. Iglesia, J. Am. Chem. Soc. 131 (2009) 6554–6565.
[61] W. Knaeble, R.T. Carr, E. Iglesia, J. Catal. 319 (2014) 283–296.
[62] A. Chica, A. Corma, Chem. Ing. Tech. 79 (2007) 857–870.
[63] C.M. Wang, R.Y. Brogaard, B.M. Weckhuysen, J.K. Nørskov, F. Studt, J. Phys. Chem. Lett. 5 (2014) 1516–1521.